Chapter 2
Models and Dynamics

This chapter describes models of distributed collector solar fields (DCSF) and uses them to discuss the typical dynamics found in these plants. The aim is not to describe a detailed model of a specific DCSF to be used for simulation purposes, as found in Camacho et al. (1988), since this would diverge from the objectives of the book. Instead, the attention is concentrated on the general dominant dynamics of DCSF plants in order to understand its structure and develop models that are adequate for adaptive control, both for algorithm design and to understand the difficulties that are to be faced by controller design.

Hence, we start by introducing a reduced complexity model that uses an energy balance to capture the spatial dependency of the system dynamics (with "space" meaning the position along the pipe) as well as on time. This model amounts to a hyperbolic partial differential equation whose solution is studied using mathematical methods and a heuristic discussion that relies on geometric arguments.

In order to prepare the ground for control algorithm development in subsequent chapters, the above infinite dimensional model is approximated to eliminate the dependency on the spatial dimension. These approximate models are an integral discrete time model obtained from the exact mathematical solution of the partial differential equation model, and continuous time state-space models obtained by projecting the spatial dependency on finite dimensional sets, either using finite differences or the orthogonal collocation method. Figure 2.1 summarizes these interdependencies between models.

The chapter concludes by making a parallel with various plants with similar dynamics, such as moisture control or glass tube manufacturing. The objective is to point out that the ideas and methods addressed throughout the book may also be applied in other types of plants.

J. M. Lemos et al., *Adaptive Control of Solar Energy Collector Systems*,
Advances in Industrial Control, DOI: 10.1007/978-3-319-06853-4_2,

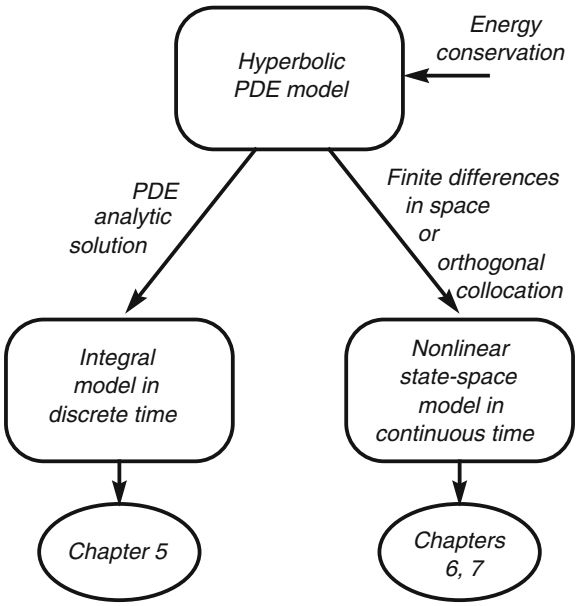

Fig. 2.1 DCSF model interdependency and the corresponding use for control design in subsequent chapters

2.1 Reduced Complexity Model

As explained in Chap. 1, the core of a DCSF is a metallic pipe inside which a working fluid, used to store energy, flows. Although the metallic pipe is inside a co-axial glass pipe used to enhance thermal efficiency by creating a greenhouse effect, this other element will not be considered in a first approach. In addition, it is assumed that there is no dependency of the fluid temperature on the radial dimension. Hence, the temperature of the fluid is described by a scalar function $T(z, t)$ where $z \in \mathbb{R}$ is a space dimension measured along the pipe, with $z = 0$ corresponding to the beginning of the pipe and $z = L$ to its maximum length, and $t \in \mathbb{R}$ is continuous time. Furthermore, it is assumed that T is the increment with respect to the environment temperature, so that $T = 0$ corresponds to the environment temperature.

In order to obtain an equation for the fluid temperature, consider the small section of the pipe between z and $z + \Delta z$, shown in Fig. 2.2. The net enthalpy accumulated in this pipe element between the time instants t and $t + \Delta t$ is given by

$$E_1 = \rho_f c_f A_f \Delta z \left[T(z, t + \Delta t) - T(z, t) \right],$$

where it is assumed that both Δt and Δz are small, ρ_f is the fluid density, c_f is the fluid specific heat, and A_f is the area of the pipe cross-section.

On the other hand, this net enthalpy is also given by the sum of two terms. One is the difference between the enthalpy entering and leaving the pipe element due to

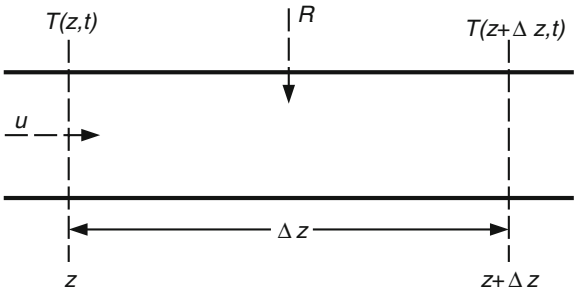

Fig. 2.2 An element of the pipe in a distributed collector solar field, and the variables used to deduce a PDE model

fluid flow, between t and $t + \Delta t$, which is given by

$$E_2 = \rho_f c_f \bar{u}(t)\Delta t \left[T(z,t) - T(z+\Delta z, t)\right],$$

where $\bar{u}$ is fluid flow. The other is the enthalpy increase due to solar energy, given by

$$E_3 = \bar{\alpha} R(t)\Delta z \Delta t,$$

where R is the solar radiation power and $\bar{\alpha}$ is a parameter related to the efficiency of energy absorption by the fluid, which depends on mirror optical efficiency and also on fluid thermal characteristics. Hence,

$$E_1 = E_2 + E_3$$

or

$$\rho_f c_f A_f \Delta z \left[T(z,t+\Delta t) - T(z,t)\right] = \rho_f c_f \bar{u}(t)\Delta t \left[T(z,t) - T(z+\Delta z, t)\right] + \bar{\alpha} R(t)\Delta z \Delta t. \tag{2.1}$$

Dividing now (2.1) by $\Delta z \Delta t$, observe that the fluid velocity u is given by

$$u = \frac{\bar{u}}{A_f}, \tag{2.2}$$

define

$$\alpha \triangleq \frac{\bar{\alpha}}{\rho_f c_f A_f}, \tag{2.3}$$

and let $\Delta t \to 0$ and $\Delta z \to 0$ to obtain the model expressed by the following partial differential equation

$$\frac{\partial}{\partial t} T(z,t) = -u \frac{\partial}{\partial z} T(z,t) + \alpha R(t). \tag{2.4}$$

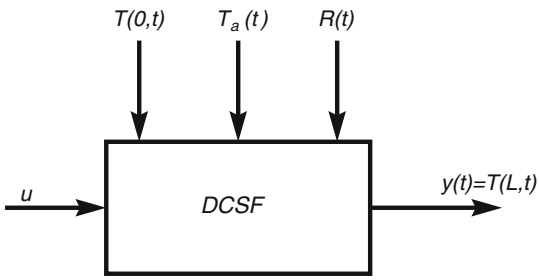

Fig. 2.3 A DCSF as a system

If heat losses to the environment are taken into account, an extra term appears and the model is given by the equation

$$\frac{\partial}{\partial t}T(z,t) = -u\frac{\partial}{\partial z}T(z,t) + \alpha R(t) - \gamma T(z,t), \tag{2.5}$$

γ is a loss coefficient. Due to the greenhouse effect created by the enveloping glass tube, the term corresponding to losses is in general less significant than the other terms. Equation (2.4) or, alternatively, (2.5), together with appropriate initial and boundary conditions, describes the dominant dynamics of a DCSF.

It is remarked that a detailed model of a DCSF build for simulation purposes must include other effects. These additions include the fact that the greenhouse effect causes an extra delay on the action of the solar radiation on the pipe. Furthermore, the specific heat c_f has a nonlinear dependence on the fluid temperature T that causes parameter α to depend on the operating point. Instead of modeling these effects, the control algorithms to follow use an approach based on parameter estimation. Furthermore, model (2.4) provides information on plant structure that is used in some of the algorithms.

2.2 Understanding the Dynamics

Figure 2.3 provides a view of a DCSF as a system. The manipulated variable input u is the fluid velocity (or, alternatively, the fuel flow), and the output $y = T(L,t)$ is the fluid temperature at the pipe outlet. There are three main disturbances, namely the fluid temperature at the pipe inlet, $T(0,t)$, the ambient temperature T_a, and the solar radiation $R(t)$. Of these disturbances, the solar radiation is the most significant due to the fast stresses it may cause, as well as for its strong and fast influence on fluid temperature. These variables are related by Eq. (2.5) or, with a further simplification, by (2.4).

The structure of the solutions of (2.4) and (2.5) is now examined. First, an exact solution is presented. Then, a qualitative discussion is made to gain insight into the type of response.

2.2.1 Exact Solution of the Distributed Model

The solution of Eq. (2.5) is defined in the plane $[z, t]$, in the set defined by $0 \leq z \leq L$ and $t \geq t_o$, where L is the length of the pipe and t_0 is the time instant in which plant operation starts. For solving (2.5), appropriate initial and boundary conditions must be defined. These conditions are the initial temperature distribution along the pipe, $T(z, t_0)$, obtained by fixing the time at the initial instant t_0, and the temperature of the fluid that enters the pipe as time passes, $T(0, t)$.

It is shown in Appendix B that the solution of Eq. (2.5) with the above initial and boundary conditions is given by

$$T(z,t) = T\left(z - \int_{t_0}^{t} u(\sigma)\,\mathrm{d}\sigma, t_0\right) e^{-\gamma(t-t_0)} + \alpha \int_{t_0}^{t} R(\sigma) e^{-\gamma(\sigma-t)}\,\mathrm{d}\sigma. \tag{2.6}$$

At this point, the reader may digress to Appendix A in order to deduce (2.6). Alternatively, the reader may proceed to follow a discussion about the properties of the solution (2.6) in Sects. 2.2.2 and 2.2.3, and then read Appendix A at a later time.

2.2.2 Qualitative Discussion

Figure 2.4 shows the plane $[z, t]$, the initial temperature distribution $T(z, t_0)$, the time evolution of the inlet fluid temperature $T(0, t)$ that is a boundary condition, and the temperature distribution along the pipe at an arbitrary time instant $t = t_1$, given by the function $T(z, t_1)$. By making the mute variable $t = t_1$, the solution formula (2.6) allows the computation of $T(z, t_1)$ as a function of $T(z, t_0)$ and $T(0, t)$.

Physical intuition tells that $T(z, t_1)$ is computed by making a shift to the right along the z-axis of the initial distribution $T(z, t_0)$ in a way that depends on the fluid flow. The left part of the pipe is filled with fluid entering through the inlet and this defines a temperature profile in this pipe section that depends on $T(0, t)$. In addition to this effect, there is a rise in temperature due to incident solar radiation, that acts in the same way in all the pipe, and that depends on the difference between t_1 and t_0. For t_0 constant, the larger the t_1 the more the radiation absorbed and the larger the impact on temperature increase.

Finally, there are losses to the environment. In the absence of solar radiation, $T(z, t_1)$ would be given not only by a shift of $T(z, t_0)$, but also by an attenuation due to

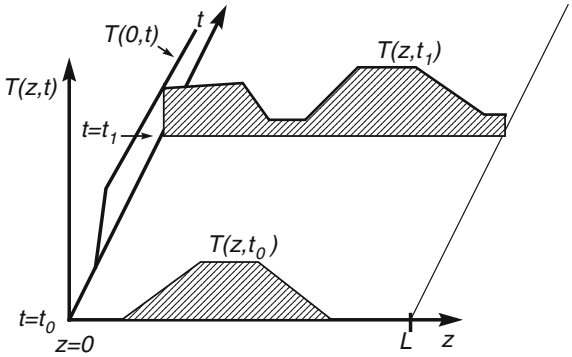

Fig. 2.4 Solution space of a DCSF with initial conditions

losses. Furthermore, when computing the cumulative effect of radiation there is also a discount factor due to losses that affects more the radiation received a longer time ago.

This physical intuition is actually confirmed by the solution (2.6). This equation computes the pipe distribution temperature $T(z, t)$ at an arbitrary instant t as the sum of two terms. The first term is

$$S_1 = T\left(z - \int_{t_0}^{t} u(\sigma)\,\mathrm{d}\sigma, t_0\right) e^{-\gamma(t-t_0)}. \tag{2.7}$$

The meaning of S_1 is the following: To compute the temperature at position z and time t, pick-up the initial distribution $T(z, t_0)$ (that is assumed to be known), shift it to the right by $\int_{t_0}^{t} u(\sigma)\,\mathrm{d}\sigma$ along the z-axis, and then attenuate it by $e^{-\gamma(t-t_0)}$, a factor that is less than 1 fot $t > t_0$.

The second term is

$$S_2 = \alpha \int_{t_0}^{t} R(\sigma) e^{-\gamma(\sigma-t)}\,\mathrm{d}\sigma \tag{2.8}$$

and its effect is to raise the fluid temperature proportionally to the integral of the radiation discounted by a factor that depends on losses. The proportionality constant α depends, among other things, on mirror efficiency.

2.2.3 Characteristic Curves

Insight into DCSF dynamics may also be obtained by examining the special case when there are neither losses nor solar radiation, in which case (2.5) reduces to

$$\frac{\partial}{\partial t} T(z, t) = -u \frac{\partial}{\partial z} T(z, t). \tag{2.9}$$

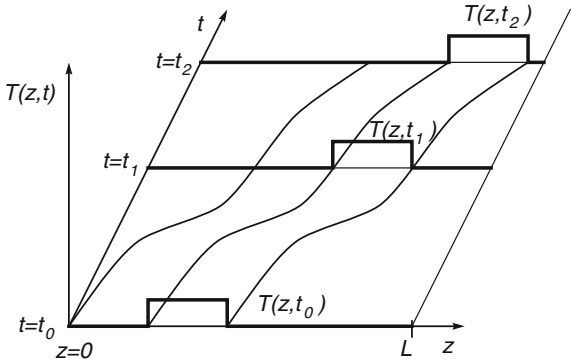

Fig. 2.5 Shift along characteristic curves of the solution of (2.9)

It is assumed in addition that the temperature of the fluid entering the pipe is $T(0, t) = 0$ at all times.

In the plane $[z, t]$ consider the curves whose coordinate z is given as a function of t by the solution of the differential equation

$$\frac{\mathrm{d}z}{\mathrm{d}t} = u \tag{2.10}$$

for various initial conditions on z. Along these curves, the solution $T(z, t)$ is constant. Indeed, along the solutions of (2.10), the total derivative of T with respect to time is, upon use of (2.10) and (2.9),

$$\frac{\mathrm{d}T}{\mathrm{d}t} = \frac{\partial T}{\partial z} \cdot \frac{\mathrm{d}z}{\mathrm{d}t} + \frac{\partial T}{\partial t} = u\frac{\partial T}{\partial z} + \frac{\partial T}{\partial t} = 0 \tag{2.11}$$

and hence it vanishes. For this reason, the solutions of (2.10) are called characteristic lines or curves and, as shown in Appendix B, they play a major role in the solution of (2.9) and also (2.5). Figure 2.5 shows an example of the solution of (2.9) obtained by propagating the initial temperature distribution along the characteristic lines.

If the flow u is constant, the solution of (2.10) is

$$z(t) = z(t_0) + u(t - t_0) \tag{2.12}$$

and the characteristic lines are straight lines. Figure 2.6 shows two situations in that the flow is constant but with different values in each case. The higher the flow the faster the temperature distribution along the pipe that affects the pipe outlet.

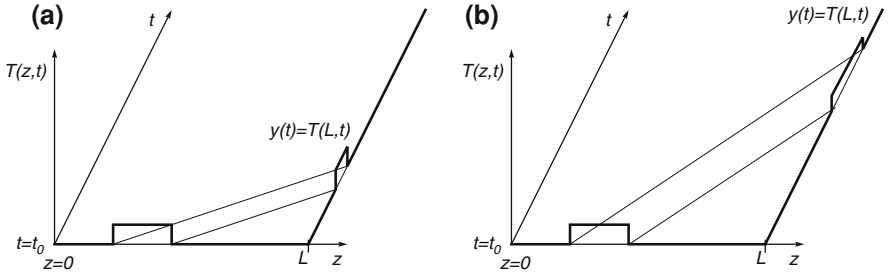

Fig. 2.6 **a** Bigger flow. **b** Smaller flow. Response of (2.9) with two different values of constant flow

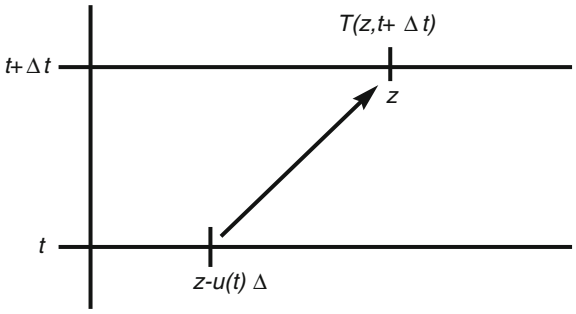

Fig. 2.7 Computing $T(z, t + \Delta t)$ from $T(z, t)$ using (2.13)

2.3 Discrete Time Integral Model

In order to obtain a discrete time integral[1] model, consider two time instants, t and $t + \Delta t$ and use the solution (2.6) to relate the respective temperature distributions. By approximating each integral in (2.6) by a rectangle, this gives

$$T(z, t + \Delta t) = T(z - u(t)\Delta t, t)e^{-\gamma \Delta t} + \alpha R(t)\Delta t \tag{2.13}$$

Equation (2.13) provides an approximate way to compute the temperature distribution at time $t + \Delta t$ from a previously known temperature distribution at time t. As shown in Fig. 2.7, to compute the temperature at position z, at time $t + \Delta t$, one should take the value of temperature at position $z - u(t)\Delta t$, at time t, multiply it by the attenuation due to losses, and then add the effect of radiation. This computation reflects the fact that the fluid is moving to the right with a velocity that, in the time interval $[t, t + \Delta t]$, is approximately $u(t)$ and, therefore, the fluid particle that was at position $z - u(t)\Delta t$ at time t moves forward to the right by a distance of $u(t)\Delta t$. Iterating (2.13) may be used to generate predictive models that are useful for control design, an approach that is explored in Chap. 5.

[1] The model is named "integral" in the sense that it is based in the integral of the PDE (2.10).

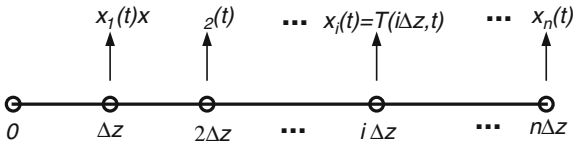

Fig. 2.8 Space grid to obtain a finite dimension state-space model of a DCSF

In a practical computation, the temperature is represented by its values in a space grid. In general, for computing $T(z, t + \Delta t)$, while z is in a grid point, $z - u(t)\Delta t$ is not, and hence $T(z - u(t)\Delta t)$ is not in the computer memory from the last iteration. One possibility to obtain $T(z - u(t)\Delta t)$ is then to approximate this quantity by interpolating the values of T at time t in neighboring points. Another possibility consists of using a varying time step Δt such that $u(t)\Delta t$ is constant and equal to the spatial grid increment Δz. As shown in Chap. 5, this option leads to predictive control algorithms with a variable time step that have the advantage of allowing fast setpoint changes without overshoot.

2.4 Finite Dimension State-Space Models

Instead of considering the fluid temperature in all the points of the pipe that lead to an infinite dimensional model, in this section we seek models in a finite dimensional state variable that is propagated in time, and from which an approximation of the temperature distribution can be recovered using algebraic operations.

2.4.1 Finite Difference Approach

One possibility is to take as state the temperature of equidistant points along the pipe. As shown in Fig. 2.8, let the points be located at $z = 0, z = \Delta z, \ldots, z = n\Delta z$, where n is the total number of points in the grid. For $i = 1, \ldots, n$, the state variable $x_i(t)$ is defined as the fluid temperature at position $i\Delta z$, according to

$$x_i(t) \stackrel{\triangle}{=} T(i\Delta z, t). \tag{2.14}$$

Using this definition, and approximating the partial derivative with respect to z using backward finite differences, by

$$\frac{\partial}{\partial z} T(z, t) \approx \frac{T(z, t) - T(z - \Delta z, t)}{\Delta z}.$$

Equation (2.5) is approximated by the set of ordinary differential equations, for $i = 2, \ldots, n$

$$\frac{\mathrm{d}x_i}{\mathrm{d}t} = -u(t)\frac{1}{\Delta z}\left((1+\gamma)x_i(t) - x_{i-1}(t)\right) + \alpha R(t). \tag{2.15}$$

In the situations considered, the temperature measured for feedback purposes is the one of the pipe outlet. Hence, the output equation is

$$y(t) = x_n(t) \tag{2.16}$$

or

$$y(t) = Cx(t), \tag{2.17}$$

where

$$C = [1\,0\,\ldots\,0]$$

and y denotes the output variable in a system framework.

For $i = 1$, Eq. (2.15) reads as

$$\frac{\mathrm{d}x_1}{\mathrm{d}t} = -u(t)\frac{1}{\Delta z}\left((1+\gamma)x_1(t) - T(0,t)\right) + \alpha R(t). \tag{2.18}$$

The inlet fluid temperature $T(0, t)$ enters Eq. (2.18) as an external signal that corresponds to a disturbance.

Defining the state vector x as the temperature along the grid points,

$$x \triangleq [x_1\ \ldots\ x_n],$$

and the parameter matrices

$$\Xi \triangleq [1\ \ldots\ 1]^T,$$

$$\overrightarrow{e}_1 = [1\,0\,\ldots\,0]^T,$$

and

$$B = -\frac{1}{\Delta z}\begin{bmatrix} 1+\gamma & 0 & \ldots & 0 \\ -1 & 1+\gamma & \ddots & \vdots \\ \vdots & \ddots & \ddots & 0 \\ 0 & \ldots & -1 & 1+\gamma \end{bmatrix}$$

the set of Eqs. (2.15), (2.18) may be written in compact form as

$$\dot{x} = Bxu + \alpha \Xi R + \overrightarrow{e}_1 \frac{u}{\Delta z} T(0,t). \tag{2.19}$$

It is remarked that matrix B is invertible and has n eigenvalues equal to $-(1+\gamma)$.

2.4.2 Reachable States

In a dynamical system such as a DCSF, the reachable states are the plant model states that can be attained, starting from the origin by manipulating the plant input within its admissible values. Characterizing the set of reachable states is of interest because it provides the ground for the control design methods based on feedback linearization that are considered in Chap. 6. In addition, this characterization shows the states that can be attained, which is important information. Indeed, the discussion made hereafter shows that, in a DCSF, when starting from a state corresponding to all fluid elements and the inlet fluid at the ambient temperature, the only possible temperature distributions along the pipe are monotonically increasing functions of space. Furthermore, for bounded fluid flow cases (as is always the case in a DCSF), the fluid temperature along the pype is also bounded.

Using methods from nonlinear dynamical systems (Nijmeijer and van der Schaft 1990; Barão et al. 2002), it is possible to show that the only directions along which the state x of the nonlinear lumped parameter model (2.19) may change are linear combinations of the three following vectors:

$$\begin{bmatrix} 1 \\ 1 \\ \vdots \\ 1 \end{bmatrix}, \quad \begin{bmatrix} 1 \\ 0 \\ \vdots \\ 0 \end{bmatrix}, \quad Bx.$$

The first vector concerns heating by solar radiation. Under constant radiation the fluid is heated uniformly along the pipe, an event that corresponds to a state trajectory aligned with the direction $\begin{bmatrix} 1 & 1 & \dots & 1 \end{bmatrix}^T$.

The second vector corresponds to the possibility of manipulating the temperature derivative with respect to space at the pipe inlet.

Finally, the third vector represents fluid transport along the pipe.

2.4.3 Jacobian Linearization

To understand the dynamics of the linearized system around an equilibrium point, assume that the radiation R is constant and that the temperature of the inlet fluid is zero, $T(0,t) = 0$. Let u_{eq} be a constant velocity of the fluid and let x_{eq} denote the corresponding value of the state at equilibrium. Both these variables satisfy

$$Bx_{\text{eq}}u_{\text{eq}} + \alpha \Xi R = 0. \tag{2.20}$$

Since B is invertible and u_{eq} is a scalar, the distribution of temperature at equilibrium can be computed explicitly by

$$x_{\text{eq}} = \frac{\alpha R}{u_{\text{eq}}} B^{-1} \Xi. \tag{2.21}$$

Let a perturbation $\Delta u(t)$ be applied to the equilibrium value. The state will respond with a variation $\Delta x(t)$ around its equilibrium x_{eq}, as well as the output y. The input and state perturbations are related by the linear matrix ODE

$$\frac{\mathrm{d}}{\mathrm{d}t}\Delta x = \left.\frac{\partial \phi}{\partial x}\right|_{\substack{x = x_{\text{eq}} \\ u = u_{\text{eq}}}} \cdot \Delta x + \left.\frac{\partial \phi}{\partial u}\right|_{\substack{x = x_{\text{eq}} \\ u = u_{\text{eq}}}} \cdot \Delta u, \tag{2.22}$$

where

$$\phi(x, u) = BXu + \alpha \Xi R. \tag{2.23}$$

Thus, the linearized model is

$$\frac{\mathrm{d}}{\mathrm{d}t}\Delta x = Bu_{\text{eq}}\Delta x + Bx_{\text{eq}}\Delta u \tag{2.24}$$

Since the output variable y is related to the state by (2.17), the corresponding increments are also related by

$$\Delta y = C\Delta x. \tag{2.25}$$

The static gain of the incremental model is obtained from (2.24) by equating the derivative to zero, yielding $-Cx_{\text{eq}}/u_{\text{eq}}$. The fact that the static gain is negative is readily interpreted in physical terms. When the flow increases, the residence time of the fluid particles inside the pipe decreases, as well as their temperature when they reach the outlet, because the particles receive less radiation.

The transfer function relating Δu with Δy is obtained by taking the Laplace transform with zero initial conditions of both sides of (2.24) and using (2.25). Observing that

$$\det(sI - Bu_{\text{eq}}) = (s + (1 + \gamma)u_{\text{eq}})^n, \tag{2.26}$$

the transfer function of the linearized system is

$$H(s) = \frac{C\,\mathrm{adj}(sI - Bu_{\text{eq}})B}{(s + (1 + \gamma)u_{\text{eq}})^n}, \tag{2.27}$$

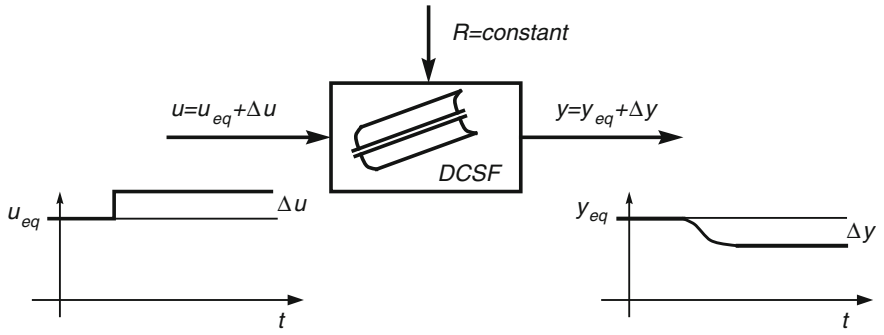

Fig. 2.9 Disturbance of an equilibrium in a DCSF

where adj denotes the adjoint of a matrix. Thus, $H(s)$ has n real and negative poles that are located at $-(1+\gamma)u_{\text{eq}}$. Since the poles are proportional to the equilibrium flow, it is concluded that the incremental response becomes faster when the flow increases. Figure 2.9 summarizes the discussion about the linearized system.

2.4.4 Orthogonal Collocation

Instead of relying on the approximation of derivatives by finite differences, the orthogonal collocation method (OCM) yields a finite dimensional approximation to the solar collector field model (2.5) by projecting the function corresponding to the exact solution $T(z,t)$ in a finite set of functions and obtaining a set of ordinary differential equations for the coefficients that express $T(z,t)$ in the basis functions (Villadsen and Michelsen 1978). This is a method commonly used in tubular and other type of chemical reactors (Dochain et al. 1992; Rice and Do 1995) that may also be used for DCSFs, with the advantage of yielding lower dimensional models than finite differences.

In order to apply the OCM to approximate (2.5) (for simplicity losses are assumed to be neglected) by a set of ordinary differential equations, it is assumed that the temperature along the pipe $T(z,t)$ is represented by the weighted sum

$$T(z,t) = \sum_{i=0}^{N+1} \varphi_i(z)\ T_i(t), \tag{2.28}$$

where $T_i(t)$ are time weights that define the state to be propagated and the functions $\varphi_i(z)$ are Lagrange interpolation polynomials, orthogonal at the so-called interior collocation points z_i for $i = 1, \ldots, N$ and at the boundary collocation points z_0 and z_{N+1}. The polynomials $\varphi_i(z)$ verify thus at the collocation points

$$\varphi_i(z_j) = \begin{cases} 1 & i = j \\ 0 & i \neq j \end{cases}. \tag{2.29}$$

Inserting (2.28) into Eq. (2.5) results in the ordinary differential equation verified by the time weights $T_i(t)$

$$\sum_{i=0}^{N+1} \varphi_i(z) \frac{\mathrm{d}T_i(t)}{\mathrm{d}t} = -\frac{u}{L} \sum_{i=0}^{N+1} \frac{\mathrm{d}\varphi_i(z)}{\mathrm{d}z} T_i(t) + \alpha R(t). \tag{2.30}$$

Compute now (2.30) at each of the collocation points $z = z_j$. Since (2.29) holds, and individuating the term $i = 0$ corresponding to the boundary conditions, it follows that

$$\frac{\mathrm{d}T_j(t)}{\mathrm{d}t} = -\frac{u}{L}\left[\sum_{i=1}^{N+1} \frac{\mathrm{d}\varphi_i(z_j)}{\mathrm{d}t} T_i(t) + \frac{\mathrm{d}\varphi_0(z_j)}{\mathrm{d}t} T_0(t)\right] + \alpha R(t). \tag{2.31}$$

By making $j = 1, \ldots, N+1$, that is to say, by considering all the collocation points apart from the first, the PDE (2.5) is therefore approximated by $n = N+1$ ordinary differential equations (ODE). The state of this nonlinear ODE system is formed of $T_i(t)$, which are the temperatures at the collocation points.

In matrix form, this lumped parameter model is written

$$\dot{x} = Bxu + \Upsilon x_0 u + \Xi \alpha R(t), \tag{2.32}$$

where

$$x = \begin{bmatrix} T_1 & T_2 & \cdots & T_{N+1} \end{bmatrix}^T, \tag{2.33}$$

is the state, with $T_i(t) = T(z_i, t)$, and z_i are the collocation points, the matrices B, Υ and Ξ are given by:

$$B = -\frac{1}{L}\begin{bmatrix} \varphi_1'(z_1) & \varphi_2'(z_1) & \cdots & \varphi_{N+1}'(z_1) \\ \varphi_1'(z_2) & \varphi_2'(z_2) & \cdots & \varphi_{N+1}'(z_2) \\ \vdots & \vdots & \ddots & \vdots \\ \varphi_1'(z_{N+1}) & \varphi_2'(z_{N+1}) & \cdots & \varphi_{N+1}'(z_{N+1}) \end{bmatrix}, \tag{2.34}$$

$$\Upsilon = -\frac{1}{L}\begin{bmatrix} \varphi_0'(z_1) \\ \varphi_0'(z_2) \\ \vdots \\ \varphi_0'(z_{N+1}) \end{bmatrix}, \qquad \Xi = \begin{bmatrix} 1 \\ 1 \\ \vdots \\ 1 \end{bmatrix}, \tag{2.35}$$

where

$$\varphi_j^{'}(z_i) \triangleq \frac{\mathrm{d}\varphi_j(z)}{\mathrm{d}z} \mid_{z=z_i} \tag{2.36}$$

and $T_0(t)$ is the boundary condition.

Equation (2.32) has the same structure as the equation that describes the finite dimensional model obtained by finite differences and given by Eq. (2.19). The main difference consists in the fact that, for the same level of the approximation error, orthogonal collocation requires a state of much smaller order than the finite difference method.

2.5 Plants with Similar Dynamics

Most of the ideas on control design discussed in this book can be applied to plants with a dynamics that is similar to that of DCSFs. In broad terms, these plants are characterized by processes with both a temporal and spatial dependence in which a fluid flows along a scalar dimension (for instance inside a pipe) and with energy exchanges along the spatial dimension. The manipulated variable is either the fluid speed or flow, or the power received along the space dimension. Furthermore, it is assumed that diffusion is negligible.

It is remarked that, although in DCSFs the manipulated variable is usually taken to be the fluid flow, it is possible to make a change in variables such as to define a virtual manipulated variable that amounts to be a correction of incident solar radiation, as shown in Chap. 5.

In mathematical problems, the plants considered are described by a Cauchy problem (Pazy 1983) associated to a hyperbolic PDE like (2.41), where a variable $T(z, t)$ that is not necessarily the temperature, evolves in time from an initial condition $Tz, 0)$, with t denoting time and $0 \leq z \leq L$ denoting the scalar coordinate of the space dimension.

The examples described hereafter that illustrate this class of plants are:

- Moisture drying
- Traffic in highways
- Glass tube manufacturing
- Air heating fan
- Steam superheaters

These examples illustrate (but by no means exhaust) the variety of plants that can be controlled with the methods described in Chaps. 2–8. Furthermore, some of them will be used to illustrate briefly the use of these methods in a context outside the DCSF area.

In addition to the above examples, control of trailing centerline in arc welding is also described. Although this process is no longer described by an hyperbolic model because, in addition to movement, there are significant diffusion effects, controller design for it can be done using the algorithms of Chaps. 3 and 4. Furthermore, the

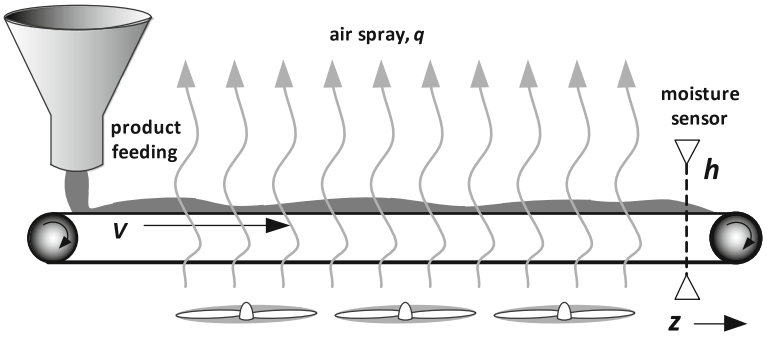

Fig. 2.10 Schematic view of a drying plant

key idea of Chap. 5 of using a sampling interval that depends on movement velocity may also be used with advantage.

2.5.1 Moisture Control

Drying is an operation frequently performed in several types of industrial processes such as those found in the pharmaceutical industry, the food industry (such as "Italian pasta manufacturing"), cereal processing, or coal preparation for use in thermoelectric power plant units. The objective is to reduce the moisture content of a given product, usually provided in the form of powder, small grains, or porous paste (Nybrant 1988; Moreira and Bakker-Arkema 1990).

Figure 2.10 shows a schematic view of a moisture drying line that consists of a conveyor belt that moves with a velocity v, and over which the material to dry is transported. At the beginning of the conveyor belt a feeder drops the product to dry in order to form a layer over the moving belt with an approximately constant thickness. In order to remove the moisture, a number of fans impel hot air through the belt with a flow $q(t)$.

Let $w(z, t)$ denote the moisture quantity per unit volume of the material spread along the belt, where z is the abscissa of a coordinate system aligned with the belt that has the origin at the feeding point and t is time. It is assumed that the rate of moisture removal is proportional to $q(t)w(z, t)$.

In order to obtain a mathematical model of this process consider a small section of the belt between the points with abscissa z and $z + \Delta z$, with Δz small. The difference between the moisture quantity inside the volume element at times t and $t + \Delta t$, where Δ is a small increment of time, is given by

$$M_1 = A_b \Delta z \left[w(z, t + \Delta t) - w(z, t) \right],$$

where A_b denotes the area of the cross section of the material over the belt.

On the other hand, the accumulation of moisture in the volume element due to the belt movement is given by

$$M_2 = A_b v \Delta t \left[w(z,t) - w(z + \Delta z, t) \right],$$

while there is a quantity of moisture leaving the element of volume that is given by

$$M_3 = \beta A_b w(z,t) \Delta z \Delta t,$$

where β is a parameter. A mass balance applied to the moisture results in

$$M_1 = M_2 + M3.$$

Dividing by $\Delta z \Delta t$ and making the increments $\Delta z \to 0$, $\Delta t \to 0$ results in the model

$$\frac{\partial}{\partial t} w(z,t) = -v \frac{\partial}{\partial z} w(z,t) - \beta q(t) w(z,t), \tag{2.37}$$

an equation similar to (2.6).

2.5.2 *Traffic in Highways*

Traffic-flow modeling and control is an area that attracts increasing attention and provides an example in which the process variable of interest is not temperature. A simple model of a unidirectional highway section with neither sinks nor sources is obtained as follows: Let $\rho(z, t)$ denote the concentration (number of vehicles per unit length) at position z of the highway and time t, and $q(z, t)$ denote the flow (number of vehicles that pass at point z per unit time. Consider an element of the highway between positions z and $z + \Delta z$ and during a time interval Δt, with both Δz and Δt small.

By the definition of ρ, the accumulation of vehicles inside the element during the time interval between t and $t + \Delta t$ is given by

$$N_1 = \Delta z(\rho(z, t + \Delta t) - \rho(z, t)).$$

On the other hand, this same quantity is also given by the number of vehicles that enter the highway element at the point with coordinate z, minus the vehicles that leave the highway element at $z + \Delta z$, that is to say

$$N_2 = \Delta t(q(z, t) - q(z + \Delta z, t)).$$

Equating N_1 and N_2, dividing by $\Delta z \Delta t$ and making the increments $\Delta z \to 0, \Delta t \to 0$ yields the conservation equation

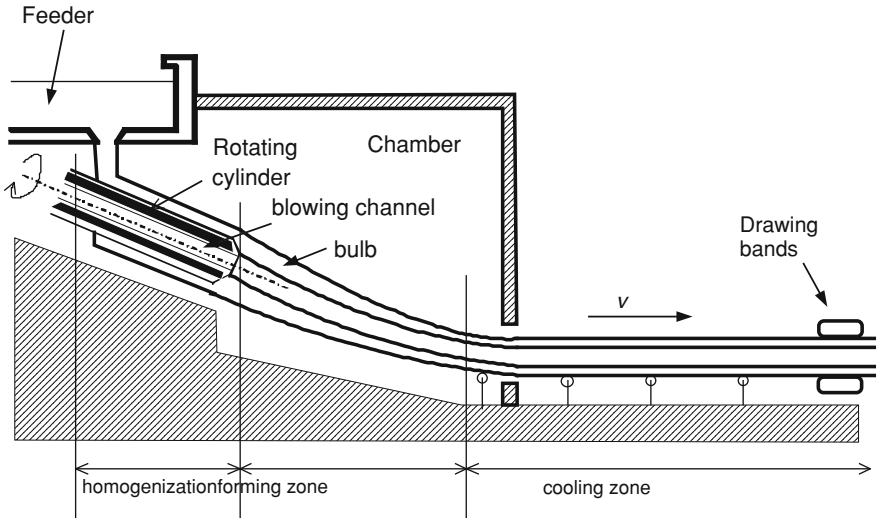

Fig. 2.11 Schematic view of the glass tube drawing bench. According to Wertz et al. (1987)

$$\frac{\partial}{\partial t}\rho(z,t) = -\frac{\partial}{\partial z}\rho(z,t). \tag{2.38}$$

Equation (2.38) can be expressed in terms of vehicle density ρ and vehicle speed u by using the relationship (Lieu 2011)

$$q(z,t) = \rho(z,t)u(z,t) \tag{2.39}$$

Using (2.39), and assuming that there are sinks/sources of vehicles, the traffic flow model reads as

$$\frac{\partial}{\partial t}\rho(z,t) = -\frac{\partial}{\partial z}\left(\rho(z,t)u(z,t)\right) + g(z,t), \tag{2.40}$$

where g is the generation dissipation of vehicles per unit length, per unit time.

2.5.3 Glass Tube Manufacturing

The glass tube drawing bench depicted in Fig. 2.11 works as follows: Molten glass drops from a feeder bowl over a tilted rotating cylinder. The air blown through an axial hole located inside the cylinder forms the tube from the glass bulb at the cylinder bottom.

Both the diameter of the tube and the thickness of its glass walls are associated to a dynamics that depends both on time and space, with the space dimension defined by

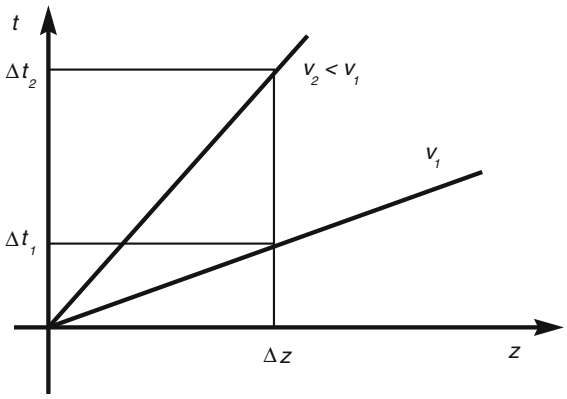

Fig. 2.12 Characteristic lines associated with glass tube movement in two different situations, corresponding to two tube constant velocities, v_1 and $v_2 < v_1$

the length along the tube. In the identification study performed in Wertz et al. (1987) the movement of the glass tube is taken into consideration by using a sampling interval that is inversely proportional to the tube velocity. This procedure can be understood by considering the simplified model of the glass movement given by

$$\frac{\partial}{\partial t} y(z,t) = -v \frac{\partial}{\partial z} y(z,t), \tag{2.41}$$

where $y(z,t)$ is the tube diameter at position z (measured along the tube) and at time t, and v is the tube velocity. Equation (2.41) is similar to Eq. (2.41) and does nothing more than to represent a shift to the right of the function $y(z,0)$ that describes the initial tube diameter along the bench. As explained in Sect. 2.2.3, this shift is such that the function $y(z,t)$ is constant along the characteristic lines in the $[z,t]$ plane, given by the solutions of the differential equation

$$\frac{\mathrm{d}z}{\mathrm{d}t} = v. \tag{2.42}$$

For constant v the general solution of (2.42) is

$$z(t) = z(0) + vt, \tag{2.43}$$

meaning that the characteristic lines are straight lines of slope v. Thus, as shown in Fig. 2.12, a point at the origin of the glass tube, moving with velocity v_1, needs a time Δt_1 to reach a point of abcissa Δz, but needs a greater time Δt_2 to reach the same point if the velocity is smaller. This means that, if the sampling interval is smaller, and if it is chosen so as to be adequate for a given velocity, it might be too big if the velocity is bigger (since the details of the dynamic response are lost), or oversampling might occur if the velocity is smaller.

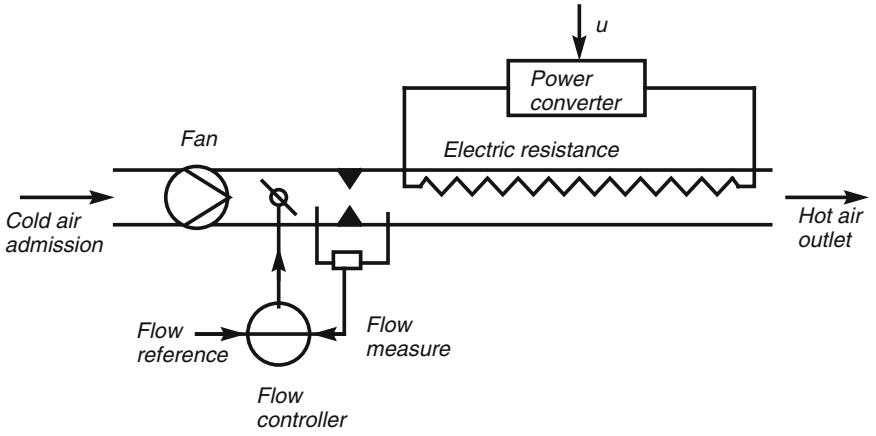

Fig. 2.13 Schematic view of the air heating fan system

Furthermore, although the transport delay of the continuous time model varies with the velocity, it becomes constant in a discrete model if the sampling time is inversely proportional to the velocity.

These observations suggest to consider the transformed timescale τ defined by

$$\tau = vt, \tag{2.44}$$

in which (2.41) reads

$$\frac{\partial}{\partial \tau} y(z, \tau) = -\frac{\partial}{\partial z} y(z, \tau), \tag{2.45}$$

The characteristic lines associated to the normalized Eq. (2.45) have a slope of 45°. This normalization is explored in Wertz et al. (1987) to obtain the same model for different tube sizes. The idea of making a normalization with respect to velocity is common to other areas such as control applications to aerospace engineering (Serra et al. 2010). This idea is also useful to design controllers for DCSFs (Silva et al. 2003a, b), as explained in Chap. 5.

2.5.4 Air Heating Fan

The air heating fan system shown in Fig. 2.13 has also a dynamical behavior that is similar to those of DCSF. This system consists of a tube inside which cold air is blown by a fan. The air flow can be adjusted with a register that is manipulated by a flow controller. Along the tube, an electric resistor liberates heat with a power that depends on the command signal (u in Fig. 2.13) of an electronic power converter. The temperature of the heated air is measured at the tube outlet.

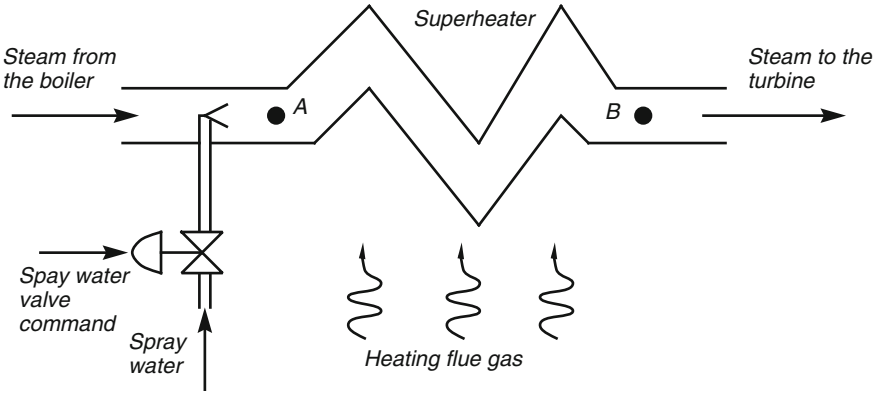

Fig. 2.14 Schematic view of the superheated steam temperature manipulation system

Neglecting diffusion, this pilot plant can be modeled by the PDE

$$\frac{\partial}{\partial t}T(z,t) = -f(t)\frac{\partial}{\partial z}T(z,t) + \alpha R(t), \tag{2.46}$$

where $T(z,t)$ is the air temperature at position z measured along the tube and at time t, $R(t)$ is the heating power and α is a parameter.

This plant is used in Chap. 4 to illustrate a control design procedure based on multiple models that is subsequently applied to a DCSF.

2.5.5 Steam Superheater

Boiler units for thermoelectric power production, either solar or with fossil fuel, include steam superheaters that have a twofold function: Eliminate the water droplets in the steam that could damage the turbine blades and increase energy use efficiency.

Associated to some superheaters there are spray water injection systems that provide a way to regulate the steam temperature at a required value (the higher as possible to maximize efficiency, but low enough to avoid damaging equipment).

Figure 2.14 shows a simplified schematic view of the so-called attemperator system, where the spray water valve is operated so as to keep the temperature of the steam leaving the superheater, at point B, close to the desired setpoint. The superheater consists of a long pipe, or parallel of pipes, inside which a fluid (steam) circulates to be heated by an external source. Up to a first approximation, the dynamics of the superheated is therefore similar to 2.46, with the velocity of response of the temperature at point B in response to a change in temperature at point A depending on steam flow.

Like the other examples in this chapter, superheated steam temperature can be controlled with the techniques described in subsequent chapters.

2.5.6 Arc Welding

In the type of arc welding considered here, the objective is to spread a seam over a workpiece (Santos et al. 2000). For that purpose, electric tension is created between a consumable electric and the workpiece that creates an electric arc. In this process, particles of the consumable electrode are liberated and form the seam over the workpiece. The consumable electrode passes through a torch that liberates a protective gas. Figure 2.15 shows a schematic view of the welding machine arrangement and Fig. 2.16 shows a photograph of the actual apparatus.

The temperature at the head point of the seam, where the arc forms, is not controllable because it corresponds to the melting temperature of the metal. Hence, the approach followed consists in measuring the temperature to be controlled 2.5 cm behind the point where the arc is formed. This means that what is controlled is the rate of cooling of the seam temperature, in what is referred in technical terms to be the trailing centerline temperature (Santos et al. 2000). This temperature is measured with a pyrometer. A screen protects the pyrometer from receiving direct radiation from the melting point. The whole set (torch, screen and pyrometer) is connected to a car that moves with a velocity that is optimized, depending on the type of materials involved and the electric tension, in order to obtain a stable arc. In the experiments reported in this book, the relation tension/car speed is optimized for the protection gas Ar–CO_2 20–80 % and the electrode made of carbon-steel ϕ 1.2 mm.

The process involves complex thermal-electro-chemical phenomena. The temperature in the workpiece can be modeled by the Fokker–Planck equation. A major difference with respect to DCSFs consists in the fact that, in arc welding, heat diffusion is much significant, resulting in a model of parabolic type. A snapshot of the space dependency of temperature at one instant of time is shown in Fig. 2.17. The shape of the isothermal curves is affected by several factors, including the car velocity and, most important, the geometric shape of the workpiece.

Hence, due to the complexity of the process it is no surprise that a high level of uncertainty affects modeling. When approximating the relationship between electric tension and temperature by a lumped parameter linear model, such as an ARX model, identified from process data, there is high variability in the model parameters when the data set changes. This is illustrated in Fig. 2.18 which shows frequency response curves corresponding to linear models identified for rectangular workpieces of the same steel, and all with the same rectangular shape, with widths of 6 and 12 mm. As it is apparent, even at low frequency there is strong variability. When considering different workpieces of different shapes and of different steels, variability is even greater and prevents the possibility of designing a single controller of constant gains to stabilize all possible plant outcomes with an acceptable performance. Thus, this example provides a good example where adaptive control may be applied with advantage.

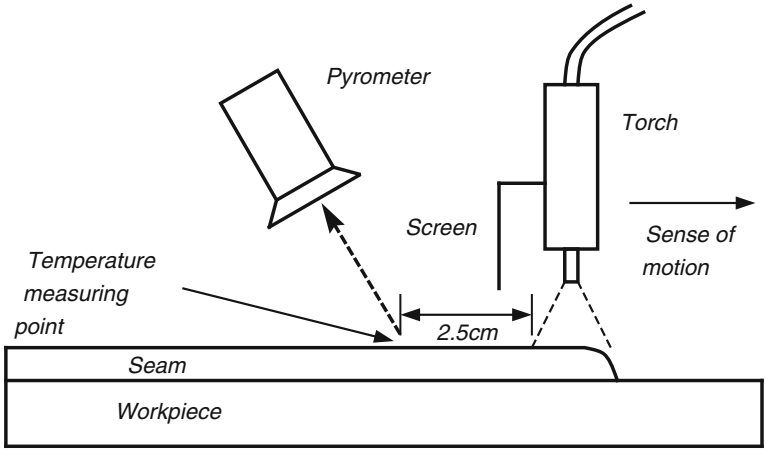

Fig. 2.15 A schematic view of the welding machine apparatus

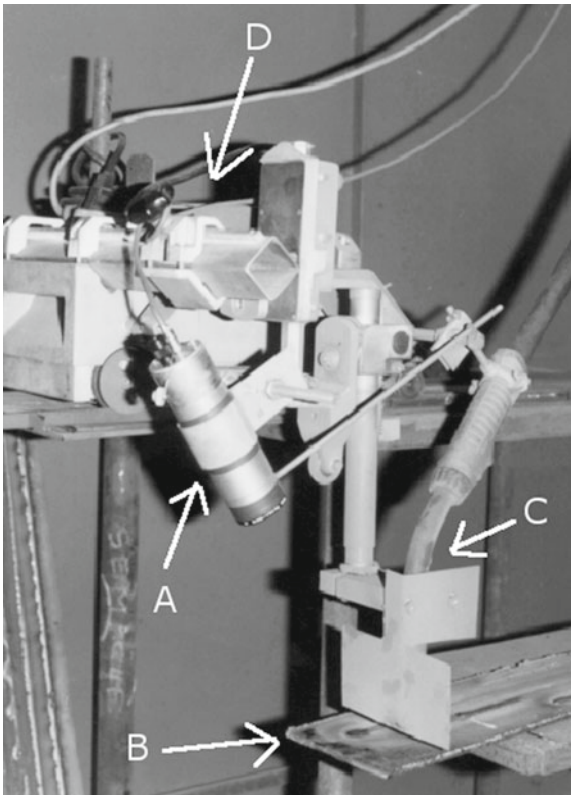

Fig. 2.16 A photograph of the welding machine setup. **a** Optical pyrometer, protected from direct radiation by a screen; **b** Plate to weld; **c** The torch, inside which passes an electrode; **d** The cart that makes the torch move

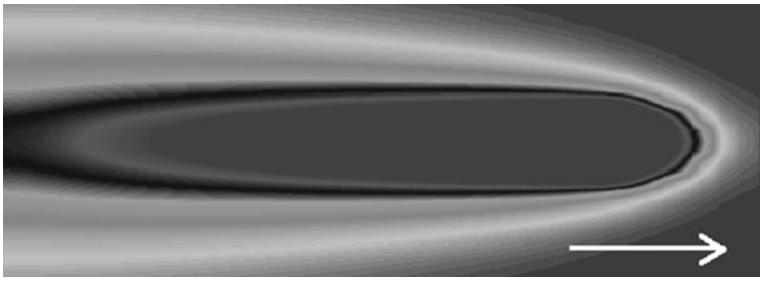

Fig. 2.17 A time snapshot of the spatial distribution of temperature in the arc welding example. The *arrow* indicates the direction of movement of the torch

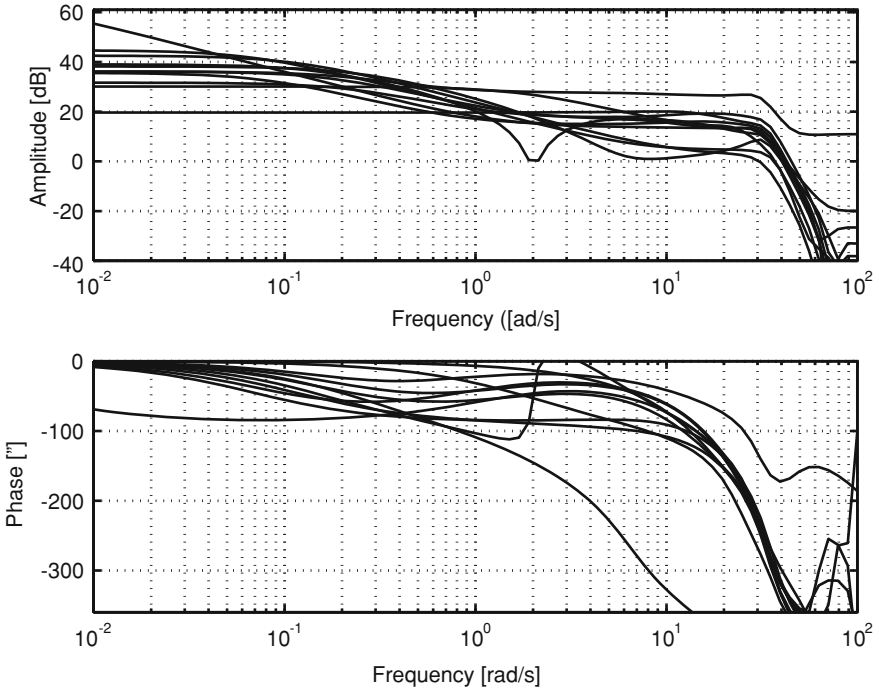

Fig. 2.18 Frequency response of transfer functions identified using different data sets between the electric tension and the temperature

2.6 Main Points of the Chapter

The dynamics of DCSF depends on space as well as on time and, as such, is represented by a PDE with appropriate initial and boundary conditions that reflect physical conditions, namely the initial distribution of fluid temperature along the pipe and fluid temperature at the inlet. The solution of this model reflects the fact that the fluid is

moving to the right, that it receives energy from solar radiation which increases its temperature, and that it is subject to thermal losses to the environment, which tends to decrease its temperature. It is possible to obtain a closed-form solution of the model and to make a numerical approximation of it resulting in a recursive model that can be used to make predictions of temperature values. In addition to this model, nonlinear state-space models with a bilinear structure are obtained in this chapter. All the models are explored in subsequent chapters in order to develop different controllers. Attention is called to the fact that the dynamics found in DCSF are common to other, seemingly different, plants that include transport phenomena and that, therefore, the ideas explored here are also useful in other system control problems, with some examples being provided.

2.7 Bibliographic Notes

A detailed model of the PSA DCSF used, which is based on physical principles and parameter estimation from plant data, is described in Camacho et al. (1988, 1997). In addition to the energy balance inside the fluid that accumulates solar radiation, the model includes an equation obtained by making an energy balance in the metal of the pipe and a nonlinear function that represents the dependence of some coefficients on temperature. A detailed review of different models is presented in Camacho et al. (2007). Bilinear state-space models are presented in Barão et al. (2002) and input/output predictive models with variable sampling in Silva et al. (2003a, b).

The solution of PDE that model processes involving mass and/or energy transport phenomena are studied in many books, some examples of which are Jeffrey (2003), Parker (2003), Grindrod (1996). The Fokker–Plank equation, which is an important model for processes that involve diffusion as well as transport and which appears in wide different areas ranging from thermal processes to telecommunications, is studied in Grindrod (1996) by using an approach that combines intuition and sound mathematical basis.

The highway traffic-flow model described is an aggregated model in the spirit of Chapter 2 of Lieu (2011). An agent-based alternative is described in Kerner and Klenov (2003), Marques and Neves-Silva (2011).

References

Barão M, Lemos JM, Silva RN (2002) Reduced complexity adaptive nonlinear control of a distributed collector solar field. J Process Control 12:131–141

Camacho EF, Rubio FR, Gutierrez JA (1988) Modelling and simulation of a solar power plant with a distributed collectors system. In: Proceedings of IFAC symposium on power systems, modelling and control applications, Brussels, pp 11.3.1–11.3.5

Camacho EF, Berenguel M, Rubio F (1997) Advanced control of solar plants. Springer, New York

Camacho EF, Rubio FR, Berenguel M, Valenzuela L (2007) A survey on control schemes for distributed solar collector fields. Part I. Modeling and basic control approaches. Sol Energy 81:1240–1251

Dochain D, Babary JP, Tali-Maamar N (1992) Modelling and adaptive control of a nonlinear distributed parameter bioreactors via orthogonal collocation. Automatica 28(5):873–883

Grindrod P (1996) The theory and applications of reaction-diffusion equations, 2nd edn. Clarendon Press, Oxford

Jeffrey A (2003) Applied partial differential equations. Academic Press, New York

Kerner BS, Klenov SL (2003) A microscopic theory of spatial-temporal congested traffic patterns at highway bottlenecks. Phys Rev E 68(3):036130

Lieu H (2011) Traffic-flow theory. Public Roads 62(4) (US Department of Transportation)

Marques M, Neves-Silva R (2011) Development of a microscopic driver-vehicle model using a control theory approach. Int J Model Simul 31(3):210–217

Moreira RG, Bakker-Arkema FW (1990) A feedforward/feedback adaptive controller for commercial cross-flow grain driers. J Agric Eng Res 45:107–116

Nijmeijer H, van der Schaft AJ (1990) Nonlinear dynamical control systems. Springer, New York

Nybrant TG (1988) Modelling and adaptive control of continuous grain driers. J Agric Eng Res 40(3):165–173

Parker DF (2003) Fields, flows and waves. Springer, New York

Pazy A (1983) Semigroups of linear operators and applications in partial differential equations. Springer, New York

Rice GR, Do DD (1995) Applied mathematics and modeling for chemical engineers. Willey, Chichester

Santos TO, Caetano RB, Lemos JM, Coito FJ (2000) Multipredictive adaptive control of arc welding trailing centerline temperature. IEEE Trans Control Syst Technol 8(1):159–169

Serra P, le Bras F, Hamel T, Silvestre C, Cunha R (2010) Nonlinear IBVS controller for the flare maneuver of fixed-wing aircraft using optical flow. In: Proceedings of 49th IEEE conference on decision and control (CDC 2010), Atlanta

Silva RN, Lemos JM, Rato LM (2003a) Variable sampling adaptive control of a distributed collector solar field. IEEE Trans Control Syst Technol 11(5):765–772

Silva RN, Rato LM, Lemos JM (2003b) Time scaling internal predictive control of a solar plant. Control Eng Pract 11(12):1459–1467

Villadsen J, Michelsen ML (1978) Solution of differential equation models by polynomial approximations. Prentice-Hall, Englewood Cliffs

Wertz V, Bastin G, Haest M (1987) Identification of a glass tube drawing bench. In: Proceedings of 10th world congress on automatic control, vol 10. IFAC, Munich, pp 334–339

Springer

http://www.springer.com/978-3-319-06852-7

Adaptive Control of Solar Energy Collector Systems

Lemos, J.M.; Neves-Silva, R.; Igreja, J.M.

2014, XXII, 253 p. 127 illus., Hardcover

ISBN: 978-3-319-06852-7